Thermodynamic profile of mutual subunit control in a heteromeric receptor

Jana Schirmeyer[a,1], Sabine Hummert[a,1], Thomas Eick[a,1], Eckhard Schulz[b,1], Tina Schwabe[a], Gunter Ehrlich[a], Taulant Kukaj[a], Melanie Wiegand[a], Christian Sattler[a], Ralf Schmauder[a], Thomas Zimmer[a], Nisa Kosmalla[a], Jan Münch[a], Michele Bonus[c,d,e], Holger Gohlke[c,d,e], and Klaus Benndorf[a,2]

[a]Institute of Physiology II, Jena University Hospital, Friedrich Schiller University Jena, 07743 Jena, Germany; [b]Faculty of Electrical Engineering, Schmalkalden University of Applied Sciences, 98574 Schmalkalden, Germany; [c]Institute for Pharmaceutical and Medicinal Chemistry, Heinrich Heine University Düsseldorf, 40225 Düsseldorf, Germany; [d]John von Neumann Institute for Computing, Jülich Supercomputing Centre, Forschungszentrum Jülich GmbH, 52425 Jülich, Germany; and [e]Institute of Biological Information Processing, Structural Biochemistry, Forschungszentrum Jülich GmbH, 52425 Jülich, Germany

Edited by Bruce P. Bean, Harvard Medical School, Boston, MA, and approved June 15, 2021 (received for review January 15, 2021)

Cyclic nucleotide-gated (CNG) ion channels of olfactory neurons are tetrameric membrane receptors that are composed of two A2 subunits, one A4 subunit, and one B1b subunit. Each subunit carries a cyclic nucleotide-binding domain in the carboxyl terminus, and the channels are activated by the binding of cyclic nucleotides. The mechanism of cooperative channel activation is still elusive. Using a complete set of engineered concatenated olfactory CNG channels, with all combinations of disabled binding sites and fit analyses with systems of allosteric models, the thermodynamics of microscopic cooperativity for ligand binding was subunit- and state-specifically quantified. We show, for the closed channel, that preoccupation of each of the single subunits increases the affinity of each other subunit with a Gibbs free energy ($\Delta\Delta G$) of ∼−3.5 to ∼−5.5 kJ · mol^{-1}, depending on the subunit type, with the only exception that a preoccupied opposite A2 subunit has no effect on the other A2 subunit. Preoccupation of two neighbor subunits of a given subunit causes the maximum affinity increase with $\Delta\Delta G$ of ∼−9.6 to ∼−9.9 kJ · mol^{-1}. Surprisingly, triple preoccupation leads to fewer negative $\Delta\Delta G$ values for a given subunit as compared to double preoccupation. Channel opening increases the affinity of all subunits. The equilibrium constants of closed–open isomerizations systematically increase with progressive liganding. This work demonstrates, on the example of the heterotetrameric olfactory CNG channel, a strategy to derive detailed insights into the specific mutual control of the individual subunits in a multisubunit membrane receptor.

heteromeric membrane receptors | concatenated cyclic nucleotide-gated channels | coupled allosteric models | Gibbs free energy | microscopic cooperativity

Functional control of receptor proteins belongs to the key processes in living cells. It is mediated by the binding of ligands to highly specific binding sites at the receptor proteins, evoking conformational changes. Because many receptor proteins are oligomers composed of either equal or homologous subunits, carrying a binding site each, receptor activation is governed by several binding steps. Taking furthermore into account that upon activation the subunits can specifically influence each other in a cooperative fashion and that the conformational changes reciprocally feed back to the binding steps (1), analyzing receptor activation is challenging.

The Monod–Wyman–Changeux (MWC) model (2) has been applied successfully to interpret cooperative processes in proteins, thereby assuming that a symmetric oligomeric protein of identical subunits performs a joint allosteric conformational change of all subunits (*SI Appendix*, Fig. S1*A*). To keep the model simple, fixed stoichiometric factors are used, leaving one equilibrium constant for ligand association (K), one constant for the allosteric conformational change ($E0$), and one fixed allosteric factor (f). The MWC model has been widely applied, ranging from hemoglobin (3) to multiple membrane receptors (4). However, for heteromeric proteins with different binding sites, this concept requires a large number of different equilibrium constants for both ligand association and the allosteric conformational change, yielding for the case of a heterotetrameric protein a heterotetrameric allosteric (HA) model with 32 Kx and 16 Ex values, respectively (*SI Appendix*, Fig. S1*B*), which seems a priori daunting for quantitative analysis.

Herein, we unraveled in such an HA model the specific subunit interaction for a heterotetrameric ion channel. We term this subunit interaction "microscopic cooperativity." Ion channels provide the unique advantage over other receptor proteins that their activation can be read out directly and with high precision by current measurements, even down to the level of single channels (5). This led to quantification of channel activation with MWC-like models in both homomeric (6–11) and, to a lesser extent, also in heteromeric channels (12, 13). MWC-like models were generally preferred because the pore opening and closure proceed in a single step. However, detailed insight into the microscopic cooperativity is still lacking, for any heteromeric channel and receptor protein as well.

Natural olfactory cyclic nucleotide-gated (CNG) channels (14, 15) are heterotetramers composed of three homolog subunits, CNGA2 (A2), CNGA4 (A4), and CNGB1b (B1b) in a stoichiometry 2:1:1 (16). Each subunit contains in the intracellular C

Significance

Membrane receptors control innumerous essential functions of living cells and are proven drug targets for pharmacological interventions. Many receptors are composed of a number of subunits and contain multiple binding sites for ligands, resulting in intricate mechanisms of subunit activation. To understand these mechanisms, the subunit action is usually modeled by allosteric schemes assuming a fixed subunit cooperativity. Here, we use subunit concatenation, binding-site mutations, and global mathematical analyses to study the interaction of the individual subunits in heterooligomeric olfactory cyclic nucleotide-gated ion channels, which are composed of three types of subunits. Our analyses provide a detailed thermodynamic profile for these interactions upon channel activation, and they can be applied to any other oligomeric ion channel and receptor.

Author contributions: J.S., T.K., M.W., and N.K. performed research; J.S., S.H., T.E., E.S., C.S., R.S., J.M., M.B., H.G., and K.B. analyzed data; S.H., T.E., E.S., and K.B. designed research; T.S., G.E., and T.Z. contributed new reagents/analytic tools; and K.B. wrote the paper.

The authors declare no competing interest.

This article is a PNAS Direct Submission.

[1]J.S., S.H., T.E., and E.S. contributed equally to this work.

[2]To whom correspondence may be addressed. Email: klaus.benndorf@med.uni-jena.de.

This article contains supporting information online at https://www.pnas.org/lookup/suppl/doi:10.1073/pnas.2100469118/-/DCSupplemental.

Published July 23, 2021.

terminus a cyclic nucleotide-binding domain (CNBD), that is linked via the C-linker to the S6 helix, contributing to the pore domain (PD).

The channels are activated by the binding of cyclic nucleotides to the CNBDs of all four subunits (17, 18). The A4 and B1b subunits (19–21) also generate specific functional effects, including an increase in the sensitivity to cyclic nucleotides (17, 22–24), a reduction of the unitary conductance (22), and the mediation of effects by Ca-Calmodulin (22, 25).

In this study, we disentangle the microscopic cooperativity of the different subunits in heterotetrameric olfactory CNG channels and calculate the thermodynamic profile of the mutual subunit interactions at equilibrium by analyzing an extended system of intimately coupled allosteric models by a global fit analysis. For a closed channel, we show that preoccupation of a single A4 and B1b subunit increases the affinity of each other subunit with Gibbs free energies of −3.5 to −5.5 kJ · mol^{-1}, whereas preoccupation of two neighbor subunits causes a much stronger affinity increase −9.6 to −9.9 kJ · mol^{-1}. Surprisingly, triple preoccupation in the closed channel causes less negative Gibbs free energies for a given subunit compared to double preoccupation, and this reduction of the negative Gibbs free energies is abolished by channel opening. Our results provide not only detailed insight into the activation mechanism of heteromeric CNG channels but also a general strategy for analyzing other oligomeric channels and receptors.

Results

We studied the microscopic cooperativity of these channels by generating a defined arrangement of the four subunits by concatenation, specifically disabling their CNBDs, and subjecting the multiple concentration dependencies of activation to a mathematical analysis with intimately coupled allosteric models.

Given one A4, one B1b, and two A2 subunits, the number of permutations of subunits within a sequence is 12 (*SI Appendix*, Fig. S2*A*). We first constructed these 12 concatamers, expressed them, and recorded currents from inside-out patches at different cGMP or cAMP concentrations (Fig. 1*A*). With cGMP, all 12 concatamers produced similar currents and concentration–activation relationships to homomeric A2 channels, thereby scattering around the relationship of nonconcatenated heteromeric wild-type (wt) channels (*SI Appendix*, Fig. S2 *B* and *D* and Table S1), indicating that the sequence of the subunits has only a minor effect on the activation gating.

To substantiate that the 12 concatamers do not assemble awkwardly in the way that A2 subunits from more than one concatamer form homomeric A2 channels, we repeated the experiments with cAMP because for this cyclic nucleotide the EC_{50} value of CNGA2 channels is essentially higher than for heteromeric channels (14). The EC_{50} values of all 12 concatamers and wt heteromeric channels were only slightly higher than for cGMP whereas the value for wt A2 channels was much higher (*SI Appendix*, Fig. S2 *C* and *D* and Table S1), ruling out a relevant awkward assembly of homomeric A2 channels.

Wild-Type and Concatenated Olfactory CNG Channels. These results allowed us to take any concatamer as representative and to systematically permute disabling of the four binding sites. We chose A4-A2-B1b-A2 (Fig. 1*A* and *SI Appendix*, Fig. S2*A*). We then disabled the binding by the point mutations R430E, R538E, and R657E in A4, A2, and B1b, respectively (18, 26). In this context, "disabled" means that ligand binding is not entirely abolished but only strongly decreased by orders of magnitude, enabling us to monitor the action of the individual subunits over a wide concentration range.

Regarding the topography, the subunits of A4-A2-B1b-A2 can be arranged, in principle, in six ways, two each of which are characterized by one specific interface arrangement Nos. 1 to 3 (*SI Appendix*, Fig. S3*A*; all viewed from the outside). Through generating structural models with the possible subunit arrangements (*SI Appendix*, Fig. S3 *B* and *C*) and energetic analysis of the subunit interfaces (*SI Appendix*, Figs. S3*D* and S12), interface arrangement #3 was identified as most favorable. Although these computations bear some uncertainty rooted in the use of static structures, a potential inaccuracy of the free energy function, and the neglect of the linker impact, they suggest that the energetics of the protein–protein interactions may impact the subunit arrangement. Note that this arrangement would be the energetically most favorable also for any other concatamer. However, the arrangement of the linkers may further be of influence if a subunit arrangement is adopted: for example, in the A4-A2-A2-B1b concatamer, arrangement #3 requires "Z"-like subunit linkages rather than clockwise or counterclockwise ones, which appears less likely with respect to the linker lengths (*SI Appendix*, Fig. S4). In the counterclockwise topography, the linker between B1b and A2 needs to half circle the structure and, thus, may interfere sterically with linkers between A2-A4 and A2-B1b (*SI Appendix*, Fig. S3*C*). By contrast, in the clockwise topography, B1b and A2 can be connected without potential interferences. Although from the length of the linkers (162 residues for A4→A2 linker, 273 residues for A2→B1b linker, 282 residues for B1b→A2 linker) and the distances to be bridged both a clockwise and a counterclockwise arrangement would be conceivable, the lack of interference leads to the suggestion that the subunits of A4-A2-B1b-A2 preferably arrange in a clockwise manner. A clockwise arrangement also matches the arrangement in the "natural" concatamers of voltage-dependent Nav1.5 (27) and Cav1.1 (28) channels, which share basic structural elements with CNG channels, like the voltage-sensor and the PD, although they are domain-swapped channels whereas CNG channels are not. Note that the rationale and the results of our analysis remain valid for both the clockwise and counterclockwise orientation of the subunits.

Building the Complex HA Model. To keep order in the subsequent mathematical analyses, we followed the systematic notation of the HA model of *SI Appendix*, Fig. S1*B*, that is, 1, 2, 3, and 4 are assigned clockwise to the left lower A4, left upper A2, the right upper B1b, and the right lower A2 wt subunit, respectively (Fig. 1*B*). Mutated (disabled) subunits were specified by an m after the number. According to the rules of a binomial distribution, this leads to 16 concatamers with different numbers of functional and disabled binding sites.

All 16 concatamers were constructed (Fig. 1*C*), and the concentration–activation relationships were determined with cGMP. We preferred cGMP to cAMP because the higher apparent affinity provided advantages with maximally disabled channels. The relationships for the nonmutated concatamer 1234 and the maximally mutated concatamer 1m2m3m4m span a concentration range of three orders of magnitude and could be fitted with a single Hill function (Eq. **1**). The relationships for the other 14 concatamers were in between and required either one Hill function (two relationships) or the sum of two Hill functions (12 relationships; Eq. **2**), resulting in total in 68 parameters for the 16 relationships (*SI Appendix*, Fig. S5 and Table S2). Together with the severe limitations of Hill functions (1), the plethora of information encoded in the 16 relationships cannot be used for any mechanistic interpretations.

To overcome this, we built one HA model for each of the 16 concatamers with 16 states (Fig. 2 and *SI Appendix*, Figs. S6–S8), coupled these models intimately and subjected them to a global fit, resulting in an HA model (Complex HA [CHA] model). Each HA model contains 32 *Kxxxx*s for either wt (black) or mutated subunits (red) ($x = 0$ for an empty subunit, $x = 1$ for a subunit to be occupied, $x = \underline{1}$ for a preoccupied subunit). To facilitate the analysis, we rearranged the 16 closed states Cxxxx of each HA model to build the corners of a four-dimensional hypercube (4DH) in which the *Kxxxx*s form the 32 edges (Fig. 3*A*). This allowed us to fit 11

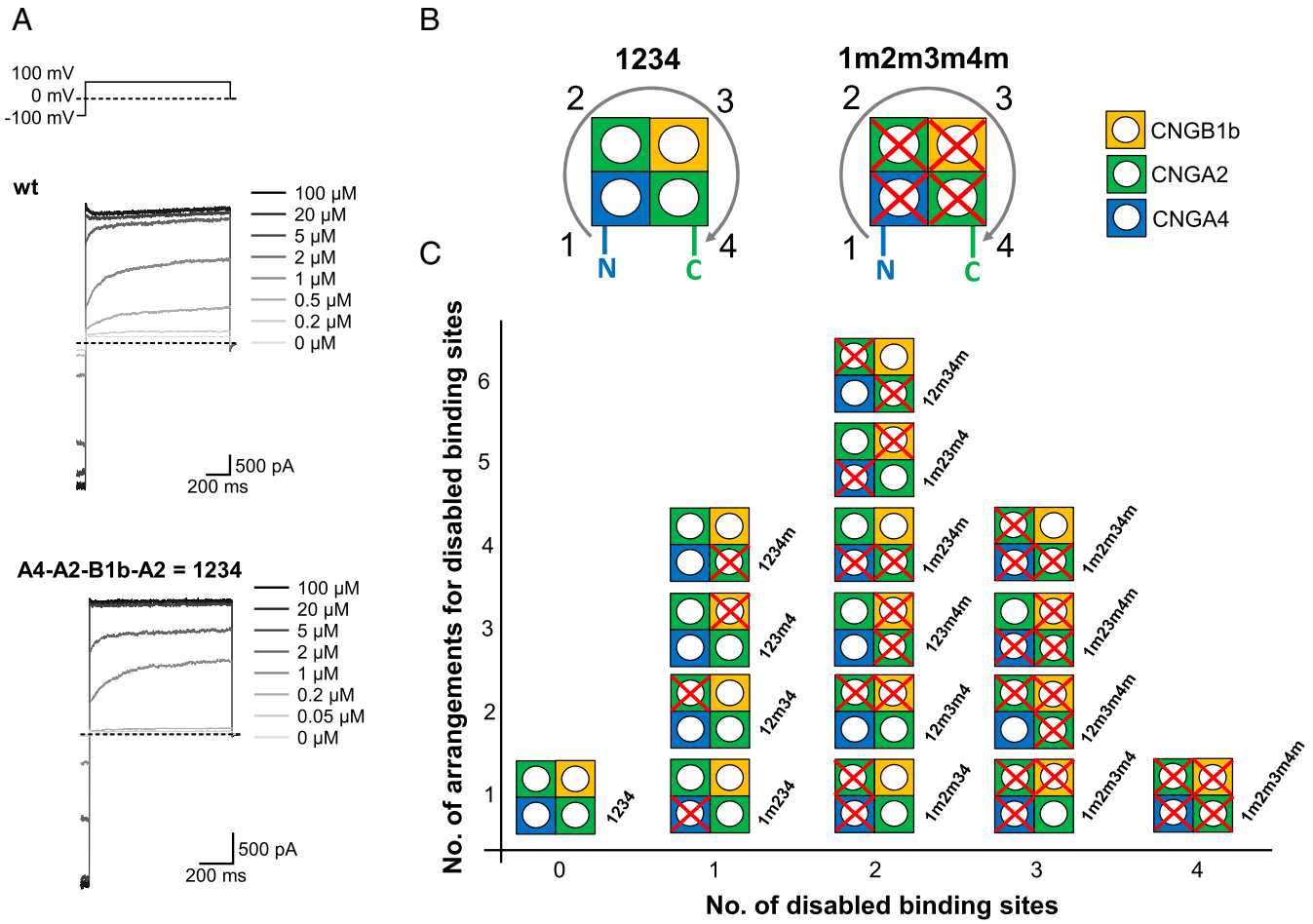

Fig. 1. The 16 A4-A2-B1b-A2 concatamers with disabled binding sites. (*A*) Two families of currents recorded from a macropatch with wt channels (*Top*) and wt concatamers A4-A2-B1b-A2 = 1234 (*Bottom*; for nomenclature, see *B*) at the indicated cGMP concentrations. (*B*) Nomenclature of the concatamers. For computations, the notation follows the subunit sequence in the concatamer A4-A2-B1b-A2 (see Fig. 2) in a clockwise direction, viewed from the outside, and corresponds to that in *SI Appendix*, Fig. S1B, that is, 1: *Lower Left* A4, 2: *Upper Left* A2, 3: *Upper Right* B1b, and 4: *Lower Right* A2. Red crosses denote disabled binding sites. (*C*) Schematic of all 16 possible concatamers with different numbers of disabled binding sites (red crosses). m after a subunit number indicates a disabled (mutated) binding site.

virtual equilibrium association constants (*Z0001* to *Z1111*) as independent parameters, to obey microscopic reversibility (29) (Fig. 3*B*), and to compute the 32 *Kxxxx*s for wt channels by respective ratios (Table 1). The global fit of the CHA model uses also three subunit-specific factors *fd* for the constants *Kxxxx* of the disabled binding sites and three equilibrium constants of the closed–open isomerizations, E_1, E_2, and E_3, resulting in 17 free parameters (see *Materials and Methods*).

Mutual Control of the Subunits Is Highly Specific. The fit with the CHA model was remarkably robust and of high quality (Fig. 3*C*), also yielding reasonable errors for the parameters (Table 1). For interpreting the interactions of the subunits, we transformed the systematic notation back to the subunit notation and plotted the *Kxxxx*s (Fig. 4 *A*–*C*) as well as factors of affinity increase, *fai*, (Fig. 4 *D*–*F*), and Gibbs free energies, $\Delta\Delta G$ (Fig. 4 *G*–*I*) derived from the *Kxxxx*s at all preoccupations with respect to the *K*s in empty channels (see *Materials and Methods*).

For the closed channel, this yielded results with highly specific effects: regarding A4 (Fig. 4 *A*, *D*, and *G*), single preoccupation of either of the two A2 neighbors (*fai* = 5.43; $\Delta\Delta G\sim-4.1$ kJ · mol^{-1}) causes a similar effect like preoccupation of the opposite B1b (*fai* = 4.42; $\Delta\Delta G\sim-3.6$ kJ · mol^{-1}). Moreover, preoccupation of both A2 neighbors causes strong cooperativity (*fai* = 50.58; $\Delta\Delta G\sim-9.6$ kJ · mol^{-1}), and there is also strong cooperativity when preoccupying B1b with either of the A2 subunits (*fai* = 22.49; $\Delta\Delta G\sim-7.6$ kJ · mol^{-1}). Regarding B1b (Fig. 4 *C*, *F*, and *I*), there is a stronger effect of the single preoccupied neighbor A2 subunits (*fai* = 10.63; $\Delta\Delta G\sim-5.7$ kJ · mol^{-1}) compared to that of the opposite A4 subunit (*fai* = 4.41; $\Delta\Delta G\sim-3.6$ kJ · mol^{-1}). Again, preoccupation of both A2 neighbors produces the most pronounced cooperativity (*fai* = 58.19; $\Delta\Delta G\sim-9.9$ kJ · mol^{-1}), which is only slightly smaller when the opposite A4 and either one of the A2 neighbors is preoccupied (*fai* = 44.00; $\Delta\Delta G\sim-9.2$ kJ · mol^{-1}). Regarding A2 (Fig. 4 *B*, *E*, and *H*), the situation differs notably from that of the other two subunits: a preoccupied B1b alone causes strong positive cooperativity for ligand binding (*fai* = 10.63; $\Delta\Delta G\sim-5.7$ kJ · mol^{-1}) while a preoccupied A4 has only half of the effect (*fai* = 5.43; $\Delta\Delta G\sim-4.1$ kJ · mol^{-1}). In contrast, the opposite A2 has no effect. Analogously, the combined preoccupation of both neighbors, A4 and B1b, causes a strong cooperative effect (*fai* = 54.12; $\Delta\Delta G\sim-9.76$ kJ · mol^{-1}), and the opposite A2 has no additional effect when combined with preoccupation of either A4 or B1b. Surprisingly, all triple preoccupations produce an affinity much below those in the respective cases of double preoccupation.

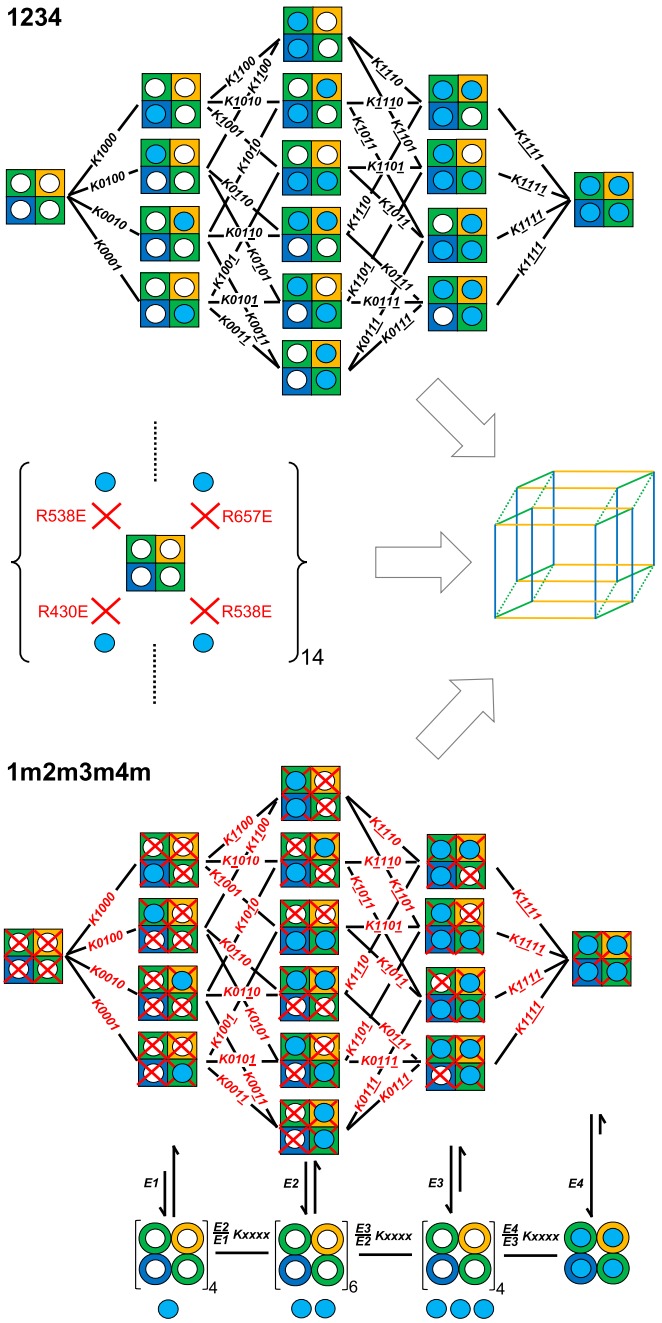

Fig. 2. The CHA model used in the global fit. HA models for the concatamers 1234 and 1m2m3m4m out of the full set of 16 HA models shown in *SI Appendix*, Figs. S6–S8. Equilibrium association constants for ligand binding, *Kxxxx* ($x = 0$ for an empty subunit, $x = 1$ for a subunit to be occupied, $x = \underline{1}$ for a preoccupied subunit), are indicated in black for a wt and red for a disabled subunit. An HA model contains 32 *Kxxxx*s, either black or red. For the CHA model consisting of 16 HA models (*SI Appendix*, Figs. S6–S8), the total number of black and red *Kxxxx*s is 64. Blue circles represent a ligand, white circles an empty binding site, and a red cross a disabled binding site. The set of closed–open isomerizations on the *Bottom* is equally valid for all HA models. For computation of the equilibrium association constants, each HA model is transformed to a 4DH (see Fig. 3 *A* and *B*).

For the three equilibrium constants of closed–open isomerizations at intermediate liganding, *E1-E3*, the values increased about five times for the second and third ligand ($E2/E1 = 5.53$; $E3/E2 = 4.36$) and about 20 times for the fourth ligand ($E4/E3 = 20.6$). Assuming transitions between the open states (Fig. 2, *Bottom*), which cannot be proven from equilibrium data, detailed balance requires that these ratios specify the affinity increase of the open versus the closed channel at the respective degree of liganding. This allowed us also to determine the amount of $\Delta\Delta G$ reduction for the assumed binding reactions in the open channel compared to the closed channel, yielding in particular a more pronounced energy sink for the quadruple occupied open versus closed channel (Fig. 4 *G–I*).

As to the specific disabling of the subunits by the mutations, our analysis yielded that A2 is significantly less disabled with $fd_2 = fd_4 = 7.49 \times 10^{-3}$ than B1b and A4 with $fd_3 = 1.10 \times 10^{-4}$ and $fd_1 = 6.86 \times 10^{-5}$, respectively (Table 1).

To demonstrate the mutual control of the subunits in a different way, we plotted for all 16 A4-A2-B1b-A2 concatamers the occupancy of the subunits versus the cGMP concentration, thereby distinguishing between the occupancy in a closed and open channel (Fig. 5). In both wt (A4-A2-B1b-A2 = 1234) and maximally disabled concatamers (A4m-A2m-B1bm-A2m = 1m2m3m4m), all four subunits become occupied at similar concentrations, leading to an only poor discrimination between the subunits. By contrast, concatamers with either one, two, or three disabled subunits generate a widely extended occupancy of the different subunits along the concentration axis with highly specific patterns. This specificity of the patterns generated substantial constraints in the global fit and, thus, enabled the highly consistent results in our analysis.

Discussion

In this study, we unraveled in unprecedented detail the microscopic cooperativity in heterotetrameric olfactory CNG channels by scaling the functional interaction of the three different subunits and employing a CHA model. Our main results for closed channels are as follows: 1) preoccupation of each of the single subunits increases the affinity of each other subunit with a Gibbs free energy $\Delta\Delta G$ of ∼−3.5 to ∼−5.5 kJ · mol^{-1}, depending on the subunit types, with the only exception that a preoccupied opposite A2 subunit has no effect; 2) preoccupation of two neighbor subunits causes the strongest increase of affinity $\Delta\Delta G$ of ∼−9.6 to ∼−9.9 kJ · mol^{-1}; 3) a strong affinity increase in B1b and A4, with $\Delta\Delta G$ of ∼−7.6 to ∼−9.2 kJ · mol^{-1}, is caused by preoccupation of one neighbor A2 plus the respective opposite A4 or B1b subunit; and 4) in the closed channel, triple preoccupation leads to less negative $\Delta\Delta G$ of a given subunit as compared to double preoccupation, an effect that is balanced by channel opening where the $\Delta\Delta G$ values are approximately similar (Fig. 4 *G–I*).

The term "cooperativity" is frequently used but only poorly defined when describing the concerted action of subunits in proteins (1). In our context, we consider microscopic cooperativity in the sense of the mutual dependence of the binding affinity of the three types of subunits in combination with allosteric channel activation.

Regarding our global fit approach with 17 free parameters, its goodness is remarkable but, at the first glance, also seems surprising. At the second glance, however, if taking into account that 16 simple concentration–activation (dose–response) relationships for proteins with interacting subunits require at least 32 free parameters (16 EC_{50} values and 16 Hill coefficients), it becomes less surprising that our approach with 16 intimately coupled HA models and 17 free parameters is so well determined. To further differentiate between the constants of the closed–open isomerizations, it is a promising idea to extend the data, for example, by other mutations or by including voltage effects, even in the case of weak voltage dependencies, and to analyze even more sophisticated systems of intimately coupled models.

When relating the functional effect evoked by the binding of a ligand to the effect evoked by the binding of the previous ligand, as for example, widely used to interpret the oxygen binding in hemoglobin (30), the second and third binding step for the B1b

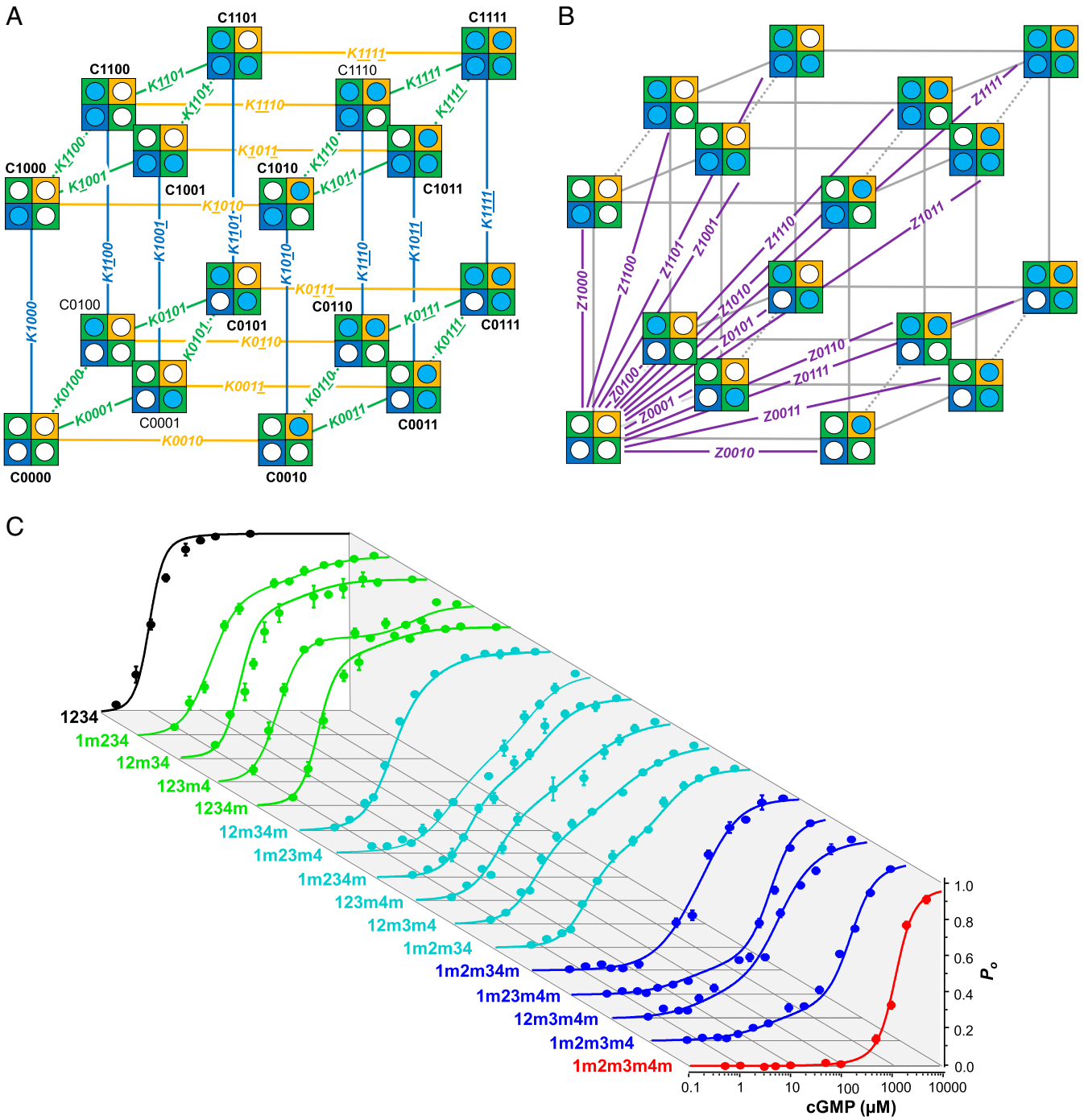

Fig. 3. Analysis of the association constants in terms of a 4DH. (*A*) The hypercube. The 16 closed states (C0000. . ..C1111) of an HA model were arranged as corners of a 4DH in which the *Kxxxxs* specify the 32 edges ($x = 0$ for an empty subunit, $x = 1$ for a subunit to be occupied, $x = \underline{1}$ for a preoccupied subunit). The blue, green, and ochre lines indicate liganding of an A4(1), A2(2,4), and B1b (3) subunit, respectively. (*B*) Virtual equilibrium association constants in the 4DH. The 15 violet lines from state C0000 to each corner indicate the 15 virtual equilibrium association constants *Z0001*. . ..*Z1111*, specifying the only independent parameters. *Z0001*. . ..*Z1111* were used to compute the 32 *Kxxxxs* for wt channels by respective ratios (Table 1). (*C*) Global fit of the concentration-P_o relationships with the CHA model shown in Fig. 2 and *SI Appendix*, Figs. S6–S8. Relationships with equal degree of liganding have the same color. For normalization of the data points, see *Materials and Methods*.

and the A4 subunit show pronounced positive cooperativity at all constellations. This contrasts to the negative cooperativity of the fourth binding step, indicated by the reduction of the respective values in the fully liganded channel. Hence, for the B1b and the A4 subunit, the cooperativity sequence is "positive – positive – negative." Regarding the A2 subunit, the second and third binding step to the B1b and A4 subunit generate also positive cooperativity, and the fourth binding step to the other A2 subunit also generates negative cooperativity (Fig. 4). However, there is no relevant cooperativity of the second and third binding step to the opposite A2 subunit.

When specifying cooperativity by relating the functional effect evoked by the binding of a cGMP always to that of the first cGMP binding step (31), the cooperativity of the fourth binding step becomes also positive. Then, binding of the fourth ligand is

Table 1. Parameters of the global fit of 16 concentration–activation relationships with the CHA model

Kxxxx	Value (mM^{-1})	s.e.m. (%)	Equal to	Genesis
K0100	4.769E+04	9.35		Z0100
K0010	2.765E+04	19.13		Z0010
K0001	4.769E+04	9.35	=*K0100*	Z0001
K1000	1.499E+05	11.19		Z1000
K0110	2.940E+05	9.93		Z0110/Z0100
K0101	5.061E+04	12.62		Z0101/Z0100
K1100	8.148E+05	9.62		Z1100/Z0100
K0110	5.069E+05	19.95		Z0110/Z0010
K0011	5.069E+05	19.95	=*K0110*	Z0011/Z0010
K1010	6.623E+05	25.20		Z1010/Z0010
K0101	5.061E+04	12.62	=*K0101*	Z0101/Z0001
K0011	2.940E+05	9.93	=*K0110*	Z0011/Z0001
K1001	8.148E+05	9.62	=*K1100*	Z1001/Z0001
K1100	2.591E+05	11.83		Z1100/Z1000
K1010	1.222E+05	20.36		Z1010/Z1000
K1001	2.591E+05	11.83	=*K1100*	Z1001/Z1000
K0111	2.770E+05	11.81		Z0111/Z0110
K1110	3.372E+06	11.11		Z1110/Z0110
K0111	1.609E+06	16.15		Z0111/Z0101
K1101	7.585E+06	15.35		Z1101/Z0101
K1110	1.217E+06	11.82	=*K1011*	Z1110/Z1100
K1101	4.712E+05	11.31		Z1101/Z1100
K0111	2.770E+05	11.81	=*K0111*	Z0111/Z0011
K1011	3.372E+06	11.11	=*K1110*	Z1011/Z0011
K1110	2.581E+06	19.94		Z1110/Z1010
K1011	2.581E+06	19.94	=*K1110*	Z1011/Z1010
K1101	4.712E+05	11.31	=*K1101*	Z1101/Z1001
K1011	1.217E+06	11.82		Z1011/Z1001
K1111	2.602E+06	11.87		Z1111/Z0111
K1111	2.137E+05	11.19		Z1111/Z1110
K1111	5.519E+05	9.92		Z1111/Z1101
K1111	2.137E+05	11.19	=*K1111*	Z1111/Z1011
E1	2.009E-01	6.35		
E2	1.110E+00	4.02		
E3	4.838E+00	4.78		
fd_1	6.858E-05	9.62		
fd_2	7.486E-03	5.25		
fd_3	1.099E-04	10.07		
fd_4	7.486E-03	5.25	=fd_2	

The equilibrium constants correspond to the schemes shown in Fig. 2 and *SI Appendix*, Figs. S6–S8 and to the fit shown in Fig. 3*C*. *Kxxxx* are given in M^{-1}; *E1 to E3* and fd_1 to fd_4 are dimensionless. The colors of the *Kxxxx* encode which of the subunits actually binds a ligand, thereby following the color specification of the subunits used throughout. The shaded rows indicate where constants were assumed to be equal. For further explanation, see *Materials and Methods*.

also facilitated by the binding of the other ligands. Only the degree of positive cooperativity varies among the different constellations and the three binding steps.

Moreover, in our HA models ligand binding with its specific cooperativity among the different subunits was intimately coupled to a single allosteric closed–open isomerization of the whole

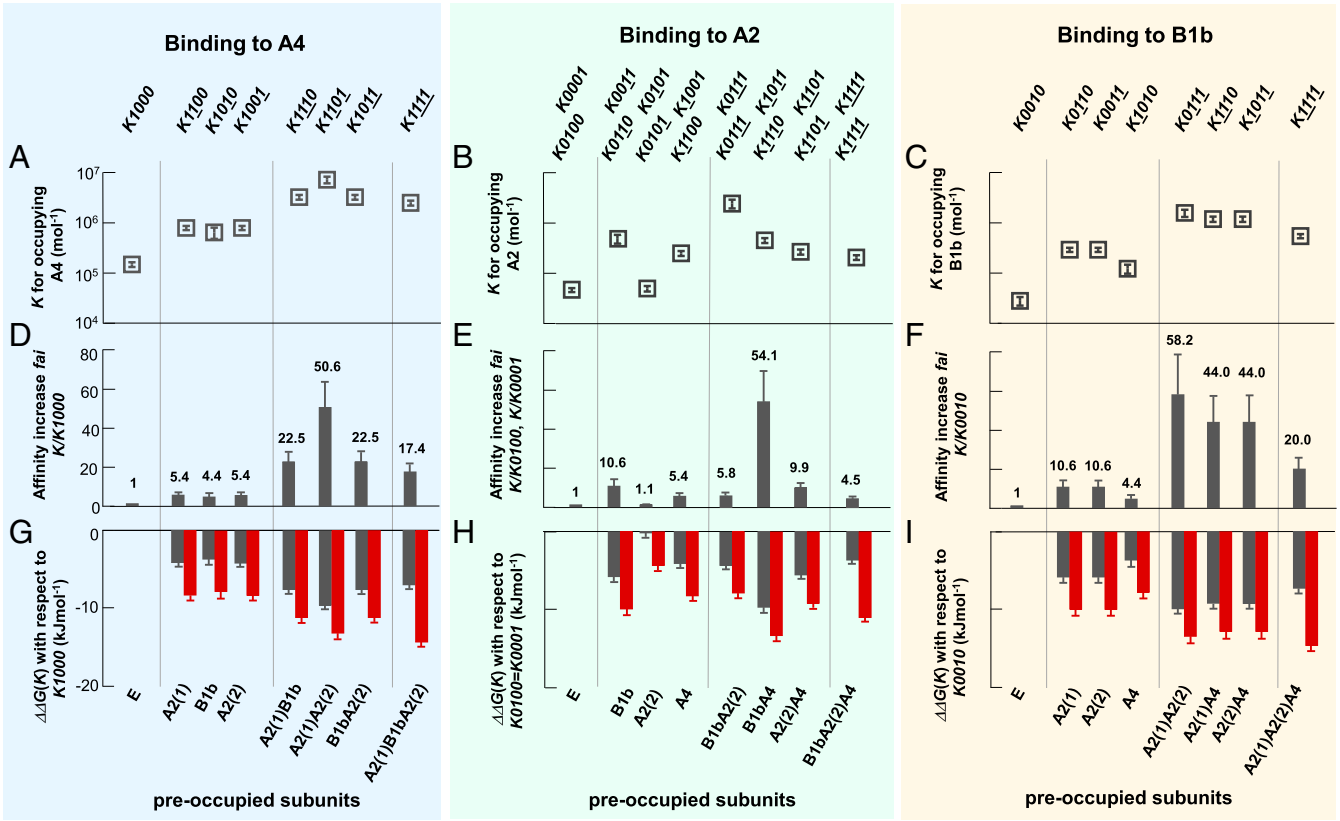

Fig. 4. Microscopic cooperativity of cGMP binding to the different subunits. (*A–C*) Equilibrium association constants of A4, A2, and B1b at different degrees of preoccupation of the other binding sites for the closed channel as specified at the bottom. "E" indicates an empty channel, that is, no subunit is preoccupied. The values correspond to Table 1. (*D–F*) Relative factors of affinity increase *fai* for the closed channel, calculated by Eq. **3**, showing how many times the affinity of a specific subunit is changed with respect to the empty subunit for each case of preoccupation of the other subunits. (*G–I*) Gibbs free energies (*ΔΔG*) of the cooperative effects. For the closed channel, the data were obtained from *fai* by Eq. **4** (gray bars). Assuming transitions between the open states, microscopic reversibility allows to calculate the *ΔΔG* values for the second, third, and fourth binding step in the open channel by multiplying the corresponding *Kxxxx* values of the closed channel with E_2/E_1, E_3/E_2, and E_4/E_3, respectively, and using Eq. **4** (red bars).

quaternary structure. This assumption was based on the single-channel data revealing the same open level at all cGMP concentrations while only the open probability, P_o, depends on the ligand concentration (*SI Appendix*, Fig. S9). This rules out models of the Koshland–Nemethy–Filmer type, which assume that the tertiary structures of the subunits are activated separately (32–34).

Another interesting aspect of our work is the question of the relation between cooperativity and asymmetry in a tetrameric channel as considered herein. It is a priori clear that a heterotetrameric olfactory channel consisting of three different subunits must have an asymmetric structure. Upon each degree of liganding, this structure can change but must stay asymmetric. Considering a homotetrameric channel, the binding of either one ligand, two ligands in cis configuration, or three ligands must also generate an asymmetric channel structure. Thus, asymmetry is definitively not an exclusive property of heterotetrameric but also of homotetrameric channels. One can generally state that the phenomenon of cooperativity per se is directly associated with asymmetry because any incomplete liganding (except double liganding in trans configuration) is associated with an asymmetric situation. Therefore, in all tetrameric proteins where cooperativity-induced steep concentration–activation or concentration binding relationships have a biological meaning, also asymmetries within the protein are involved.

To further substantiate that the results of mutations in the concatamer A4-A2-B1b-A2 selected herein are not specific for this concatamer, we compared for the concatamer A4-B1b-A2-A2, differing by the subunit sequence, the effect of two respective mutations on the concentration–activation relationship, that is, A4-A2m-B1bm-A2 versus A4-B1bm-A2m-A2 (*SI Appendix*, Fig. S13). Both relationships are closely similar, indicating that the contribution of the subunits to the activation gating is largely independent of their relative position in the sequence. These results also match previous results with homotetrameric concatamers of CNGA2 or HCN2 channels with disabled binding sites (35, 36) and support the notion of additive effects of the liganded subunits on the rotation of the tetrameric CNBD.

In conclusion, our approach provides detailed insights into microscopic cooperativity of the subunit operation in heterotetrameric CNG channels. In principle, it can be transferred to ion channels with any stoichiometry and, beyond, also metabotropic membrane receptors, if only disabling of defined binding sites is possible and receptor activation can be read out with sufficient precision.

Materials and Methods

Molecular Biology and Functional Expression. The heterotetrameric concatamers assembling to olfactory CNG channels were obtained by joining the coding sequences of two CNGA2 (accession no. AF126808) subunits, one CNGA4 (accession no. U12623) and one CNGB1b (accession No. AF068572) subunit from the rat via the short linker sequence GSA similar to the constructs for CNGA2 homotetramers (35). The 12 different arrangements (*SI Appendix*, Fig. S2A) were constructed using recombinant PCR techniques and subcloning with flanking restriction sites in front of a T7 promoter in a pGEMHEnew vector. The point mutations R538E (CNGA2), R430E (CNGA4),

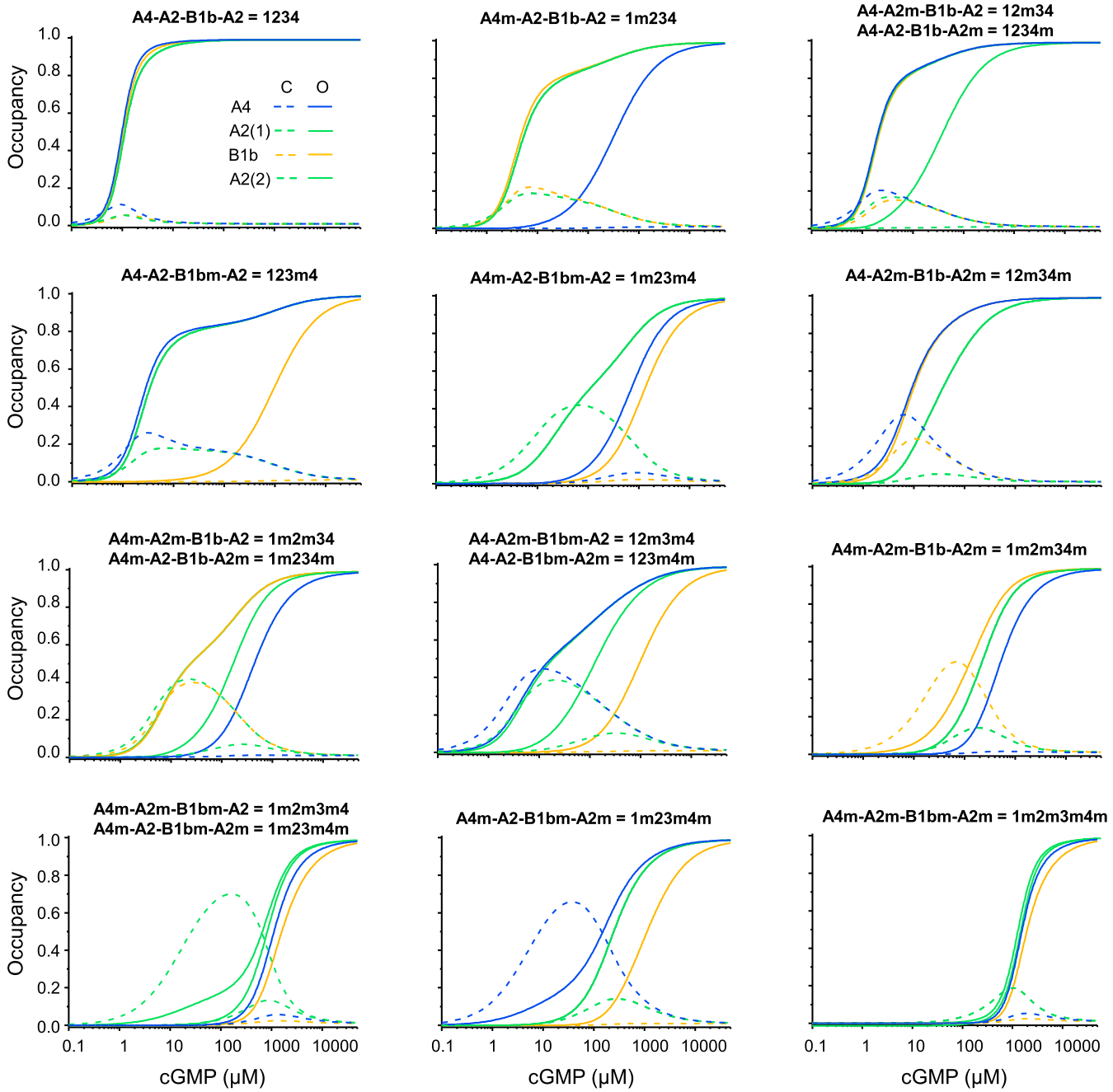

Fig. 5. Occupancy of the subunits as function of the cGMP concentration. The set of constants obtained by the global fit with the CHA model (Table 1) was used to simulate the occupancy at each subunit of the 16 concatamers 1234 through 1m2m3m4m. Blue, green, and ochre curves denote the occupancy at the A4 subunit, the two A2 subunits, and the B1b subunit, respectively. Subunits in open channels are indicated by continuous curves and in closed channels by stippled curves.

and R657E (CNGB1b) were introduced via the overlapping PCR technique, yielding all 16 combinations in the A4-A2-B1b-A4 concatamer. Correctness of the plasmids was confirmed by restriction analysis and DNA sequencing of PCR derived fragments in the open reading frame. Preparation of cRNA (coding ribonucleic acid) was done using the mMESSAGE mMACHINE T7 Kit (Ambion) after plasmid linearization with NotI.

Oocytes were harvested surgically under anesthesia (0.3% 3-aminobenzoic acid ethyl ester) from adult females of *Xenopus laevis* (37). The procedures had the approval of the authorized animal ethical committee of the Friedrich Schiller University Jena. The methods were carried out in accordance with the approved guidelines. The oocytes were digested with collagenase A (3 mg/mL, Roche) for 105 min in Ca^{2+}-free Barth´s solution containing (in mM) 82.5 NaCl, 2 KCl, 1 $MgCl_2$, 5 Hepes, pH 7.5. Oocytes of stage IV and V were manually dissected and injected with ~50 ng of cRNA encoding the respective channels. The oocytes were cultured at 18 °C for 1 to 3 d in Barth's solution containing (in mM) 84 NaCl, 1 KCl, 2.4 $NaHCO_3$, 0.82 $MgSO_4$, 0.41 $CaCl_2$, 0.33 $Ca(NO3)_2$, 7.5 Tris, Cefuroxim, Penicillin/Streptomycin, pH 7.4.

Electrophysiology. For obtaining concentration–activation relationships at equilibrium, ensemble (macroscopic) currents, generated by hundreds to several thousands of channels, were recorded from inside-out patches with a standard patch-clamp technique. The amplitude of the late current at +100 mV was evaluated. The patch pipettes were manufactured by pulling quartz tubing (VITROCOM) on a P-2000 puller (Sutter Instrument). The outer

and inner diameter of the tubing was 1.0 and 0.7 mm. The pipette resistance was 0.5 to 1.7 MΩ. Both bath and pipette solution contained the following (in mM): 150 KCl, 1 EGTA, 10 Hepes (pH 7.4 with KOH). Recording was performed with either an Axopatch 200B amplifier (Axon Instruments), controlled by the ISO2 hard- and software (MFK), or with an EPC10 amplifier and the Patchmaster software (HEKA GmbH). The sampling rate was either 2 or 5 kHz, and the internal filter of the amplifier was set to either 1 or 2 kHz.

For single-channel measurements, the patch pipettes were fabricated from quartz tubing with an outer and inner diameter of 1.0 and 0.5 mm, respectively (VITROCOM). The pipette resistance was 5.0 to 12.0 MΩ. The pipette solution contained the following (in mM): 150 KCl, 1 EGTA, 5 Hepes (pH 7.4 with KOH). The recording voltage was +100 mV. The data were recorded at 100 mV in the inside-out patch configuration at different cGMP concentrations. Recordings from wt heteromers were sampled at 20 kHz and filtered to 5 kHz on line. All other recordings were sampled at 40 kHz and filtered to 10 kHz on line. For display, the data were off-line filtered to 1 kHz by a Gaussian filter. Amplitude histograms were built from 10-s intervals and fitted with the sum of two normalized Gaussian functions from which the open probability, P_o, and the amplitude of the unitary current, i, were obtained.

Data Analysis. Concentration–activation relationships were fitted with IgorPRO 7 by the following equation:

$$I/I_{max} = 1/\left(1 + (EC_{50}/[CN])^{n}\right). \quad [1]$$

I denotes the actual current amplitude and I_{max} the maximum current amplitude at saturating cyclic nucleotide CN specified for each patch. EC_{50} is the CN concentration evoking half maximum current and n the Hill coefficient.

Part of the concentration–activation relationships required the sum of a high (H) and a low affinity (L) component:

$$I/I_{max} = A/\left(1 + (EC_{50,H}/[cGMP])^{nH}\right) + (1 - A)/\left(1 + (EC_{50,L}/[cGMP])^{nL}\right). \quad [2]$$

The notation corresponds to that in Eq. **1**. A is the fraction of the high affinity component.

To illustrate how many times the affinity of a subunit is increased by the preoccupancy of the other subunits, effects on microscopic affinity are illustrated by the relative factors of affinity increase, *fai* (Fig. 4 *D–F*), with respect to *Kyyyy* of the empty channel according to the following equation:

$$fai = Kxxxx/Kyyyy. \quad [3]$$

Kxxxx is an equilibrium association constant. *Kyyyy* is *K1000* for A4, *K0100* for A2 (1), *K0010* for B1b, and *K0001* for A2 (2).

To demonstrate the cooperative effects also in terms of energies, these values were translated to Gibbs free energies ($\Delta\Delta G$) by the following equation:

$$\Delta\Delta G = -RT(lnfai) \quad [4]$$

(Fig. 4 *G–I*). R and T are the molar gas constant and the absolute temperature in K.

Data are given as mean ± SEM.

Structural Modeling and Energetic Analysis of Subunit Interfaces. Structural models for subunit arrangement Nos. 1 to 3 were generated using RosettaCM (38) and the RosettaMP framework for membrane proteins (39). The cryo-electron microscopy structure of tax-4 (Protein Data Bank [PDB] ID: 5H3O) (40) and the CLZ domain of CNGA3 (PDB ID: 3SWY) (41) served as template structures. Interfaces were scored pairwise with the InterfaceAnalyzer program implemented in Rosetta. Reference *SI Appendix*, Supplementary Methods for further details.

The Global Fit. One assumption in our global fit was that the cGMP concentration controls exclusively P_o, that is, the gating, but not the amplitude of the unitary current, that is, the channel conductance (*SI Appendix*, Figs. S8 and S9). This confines the analysis to channel gating. Each of the 16 allosteric models in *SI Appendix*, Figs. S6–S8 for channel gating contains 32 *Kxxxx*s for either wt (black) or mutated subunits (red), resulting for all 16 models in 64 different *Kxxxx*s. These 64 *Kxxxx*s specify the 512 binding steps in the 16 HA models and generate thus both a multifaceted and intimate coupling of these models. A further assumption was that the two A2 subunits are functionally equal as suggested by the closely similar concentration–activation relationships in the four pairs of concatamers differing only by the position of the mutated A2 subunit (4212m-42m12, 4m212m-4m2m12, 421m2m-42m1m2, 4m21m2m-4m2m1m2; *SI Appendix*, Fig. S2).

For computations, we adopted the assumption that microscopic reversibility (29) is obeyed, resulting for a 16-state model in 15 independent *Kxxxx*s, while the others must be given by cycles (42). In an attempt to facilitate the computations, we interpreted the 16 closed states of our HA models as corners of a 4DH in which the transitions, specified by the *Kxxxx*s, form the 32 edges (Fig. 3*A*). Given state 0000, this enabled us to immediately determine 15 virtual equilibrium association constants (violet lines *Z0001* to *Z1111* in Fig. 3*B*) and to compute the 32 *Kxxxx*s by respective ratios (Table 1), and microscopic reversibility automatically holds (Fig. 3*B*). Assuming furthermore that at a given liganding of A4 and B1b, the two A2 subunits identical by sequence are also functionally identical (i.e., *Z0001* = *Z0100*; *Z0011* = *Z0110*; *Z1001* = *Z1100*; *Z1011* = *Z1110*), then the number of independent *Kxxxx*s reduces from 15 to 11. For disabling the binding sites, we assumed that the affinity of the same type of subunit is reduced by the same specific factor fd_y, independent of the liganding of the other subunits, resulting with $fd_2 = fd_4$ in three additional free parameters. For the equilibrium constants of the closed–open isomerizations, *Ex* (x = 0…4) (Fig. 2, *Bottom*), the following assumptions were adopted: 1) because at zero ligand we could not detect trustable single-channel activity, *E0* was set to zero; 2) for one, two, or three bound ligands, *Ex* (x = 1…3) was set equal, independent of the type of the liganded subunits, resulting in three further free parameters; and 3) *E4* for saturating cGMP was estimated in single-channel experiments on 1234 at 100 μM from P_o being 0.99 and set for all concatamers. For 1m2m3m4m and the triple mutated concatamers with one WT A2 subunit, we noticed that at our highest cGMP concentration of 5 mM P_o was slightly below saturation. A lower P_o of 0.95, determined for 1m2m3m4, and 0.92, determined for 1m2m3m4m, both at 5 mM (*SI Appendix*, Fig. S10), was obtained from single-channel experiments and all other data points of the respective concentration–activation relationships were normalized with respect to these values. The total number of free parameters for the global fit of the 16 concatamers was then 15 − 4 + 3 + 3 = 17.

The arrangement of the N = 16 closed states Cx ≡ Cijkl in the corners of a 4DH enables indexing by a 4D vector with binary values i, j, k, and l equal to either 0 or 1. The 32 edges of the hypercube correspond to the 32 possible binding events among the closed states, generating a transition from state Cx to state Cy with the equilibrium constant *Kxy*. Their binary indices differ only in one position. To gain a unique notation in the single four-dimensional vector, we denote the occupation of the actual state by '1' and pre-occupied states by '1'. For example, a transition from Cx ≡ C1001 to Cy ≡ C1011 has the equilibrium constant $Kxy \equiv K\underline{1}011$. The variable p_c0000 is the equilibrium occupation probability of the unliganded closed state C0000. Then, the occupation probability p_cijkl of each other closed state Cijkl can be easily determined with the help of virtual equilibrium constants *Zijkl*:

$$p_cijkl = p_c0000 \cdot Zijkl \cdot fd_1^a \cdot fd_2^b \cdot fd_3^c \cdot fd_4^d \cdot L^{i+j+k+l}. \quad [5]$$

The ligand concentration L appears as the power of the sum of the indices, which can adopt a maximum value of 4. The factors of disabling by mutation fd_u (u = 1,…, 4) of the four subunits have the exponents *a, b, c, d* (equal to 0 or 1) . An exponent is equal to 1 if the subunit u is mutated and has bound a ligand. Otherwise, the exponent is 0.

The occupation probability of an open state Ox ≡ Oijkl is obtained by multiplication of p_cijkl with one of the associated opening equilibrium constants E_α (α = 0,…,4) in the following form:

$$p_oijkl = p_c0000 \cdot Zijkl \cdot fd_1^a \cdot fd_2^b \cdot fd_3^c \cdot fd_4^d \cdot L^{i+j+k+l} \cdot E_{i+j+k+l}. \quad [6]$$

For an effective notation, we define five subtotals S_α:

$$S_\alpha = \sum_{i+j+k+l=\alpha} \left(Zijkl \cdot fd_1^a \cdot fd_2^b \cdot fd_3^c \cdot fd_4^d\right), \quad [7]$$

where the summation extends over all combinations of i, j, k, l with the same sum α = 0, …, 4.

Then the open probability P_{oc} *(L)* of the whole channel can be calculated according to the following:

$$P_{oc}(L) = \left(\sum_{\alpha=0}^{4} E_\alpha S_\alpha L^\alpha\right) \cdot \left(\sum_{\alpha=0}^{4} (1 + E_\alpha) S_\alpha L^\alpha\right)^{-1}. \quad [8]$$

The squared differences between the calculated and the measured open probabilities P_{om} *(L)* are added up to χ^2:

$$\chi^2 = \sum_{k=1}^{n_c} \sum_{i=1}^{n_k} \frac{\left(P_{om}(L_{k,i}) - P_{oc}(L_{k,i})\right)^2}{\sigma_{k,i}^2}. \quad [9]$$

The summation covers all $n_c = 16$ concatamers, that is, HA models, at the respective n_k concentrations. The weighting factors are the reciprocal of the empirical variances $\sigma_{k,i}^2$ of the mean, which have been estimated from measurements in 6 to 18 patches. Minimization of χ^2 was performed with the Levenberg–Marquardt algorithm (43). This provides the 11 virtual equilibrium constants *Zijkl*, the 3 factors of disabling by mutation fd_1, $fd_2 = fd_4$, fd_3, and the opening constants E_1, E_2, E_3. In addition, a 17×17 covariance matrix COV of the 17 fitted parameters is obtained. The actual equilibrium association constants *Kxy* for the second, third, and fourth binding step to a nonmutated subunit are calculated simply by

$$Kxy = Zy/Zx\,, \quad [10]$$

yielding, for example, *K1011=Z1011/Z1001*. In the four special cases of the first binding step, the actual equilibrium association constants *Kxy* are directly given by $Ky = Zy$. The SD σ_{Kxy} of an equilibrium constant *Kxy* calculated in this way is obtained using the error propagation formula for correlated input variables (43).

$$\sigma_{Kxy} = \sqrt{J \times \mathrm{COV}_{xy} \times J^T}\,, \quad [11]$$

with the Jacobian matrix $J = \left(\frac{\partial Kxy}{\partial Zx}\ \frac{\partial Kxy}{\partial Zy}\right)$ and the 2×2 matrix COV_{xy}, consisting of the rows and columns x and y of COV, respectively.

When a ligand binds to a mutated subunit u, *Kxy* is calculated according to the following:

$$Kxy = fd_u \cdot Zy/Zx\,. \quad [12]$$

In the schemes, *Kxy* for binding steps to disabled subunits are indicated by red color. For these binding steps to disabled subunits, the error of the factor fd_u must also be included in the error of *Kxy*. According to Eq. **11**, the error is obtained according to the rules of error propagation by using the Jacobian matrix $J = \left(\frac{\partial Kxy}{\partial Zx}\ \frac{\partial Kxy}{\partial Zy}\ \frac{\partial Kxy}{\partial fd_u}\right)$ and the 3×3 matrix COV_{xyu}, which contains additionally the associated row and column of COV belonging to fd_u.

To further validate the quality and the robustness of the 17-parameter global fit beyond determining χ^2 and the unexpectedly high precision of the parameters, we repeated the global fit 2,000 times with stochastically varied values of the starting vector (*SI Appendix*, Fig. S11). The result was that the fit went 1,952 times into the global minimum with $\chi^2 = 697.01$. The remaining 48 fits could be ruled out by at least 2.5 times higher χ^2 values.

Data Availability. Custom Matlab code and data used for the global fit have been deposited in Open Science Framework (https://osf.io/8jdtw/). All other data are included in the manuscript and/or *SI Appendix*.

ACKNOWLEDGMENTS. We thank G. Ditze, G. Sammler, F. Horn, M. Händel, K. Schoknecht, S. Bernhardt, C. Ranke, and A. Kolchmeier for technical assistance. This work was supported by the Research Unit 2518 DynIon (project P2 to K.B. and P7 to H.G.) and the Collaborative Research Center Transregio 166 ReceptorLight (project A5 to K.B.) of the Deutsche Forschungsgemeinschaft.

1. D. Colquhoun, Binding, gating, affinity and efficacy: The interpretation of structure-activity relationships for agonists and of the effects of mutating receptors. *Br. J. Pharmacol.* **125**, 924–947 (1998).
2. J. Monod, J. Wyman, J.-P. Changeux, On the nature of allosteric transitions: A plausible model. *J. Mol. Biol.* **12**, 88–118 (1965).
3. W. A. Eaton, E. R. Henry, J. Hofrichter, A. Mozzarelli, Is cooperative oxygen binding by hemoglobin really understood? *Nat. Struct. Biol.* **6**, 351–358 (1999).
4. J.-P. Changeux, S. J. Edelstein, Allosteric mechanisms of signal transduction. *Science* **308**, 1424–1428 (2005).
5. O. P. Hamill, A. Marty, E. Neher, B. Sakmann, F. J. Sigworth, Improved patch-clamp techniques for high-resolution current recording from cells and cell-free membrane patches. *Pflugers Arch.* **391**, 85–100 (1981).
6. B. Keceli, Y. Kubo, Signal transmission within the P2X2 trimeric receptor. *J. Gen. Physiol.* **143**, 761–782 (2014).
7. V. Nache, T. Eick, E. Schulz, R. Schmauder, K. Benndorf, Hysteresis of ligand binding in CNGA2 ion channels. *Nat. Commun.* **4**, 2866 (2013).
8. J. Kusch *et al.*, How subunits cooperate in cAMP-induced activation of homotetrameric HCN2 channels. *Nat. Chem. Biol.* **8**, 162–169 (2011).
9. J. H. Steinbach, G. Akk, Applying the Monod-Wyman-Changeux allosteric activation model to pseudo-steady-state responses from $GABA_A$ receptors. *Mol. Pharmacol.* **95**, 106–119 (2019).
10. A. Auerbach, Thinking in cycles: MWC is a good model for acetylcholine receptor-channels. *J. Physiol.* **590**, 93–98 (2012).
11. M. Beato, P. J. Groot-Kormelink, D. Colquhoun, L. G. Sivilotti, The activation mechanism of alpha1 homomeric glycine receptors. *J. Neurosci.* **24**, 895–906 (2004).
12. V. Burzomato, M. Beato, P. J. Groot-Kormelink, D. Colquhoun, L. G. Sivilotti, Single-channel behavior of heteromeric alpha1beta glycine receptors: An attempt to detect a conformational change before the channel opens. *J. Neurosci.* **24**, 10924–10940 (2004).
13. R. Lape, D. Colquhoun, L. G. Sivilotti, On the nature of partial agonism in the nicotinic receptor superfamily. *Nature* **454**, 722–727 (2008).
14. U. B. Kaupp, R. Seifert, Cyclic nucleotide-gated ion channels. *Physiol. Rev.* **82**, 769–824 (2002).
15. W. N. Zagotta, S. A. Siegelbaum, Structure and function of cyclic nucleotide-gated channels. *Annu. Rev. Neurosci.* **19**, 235–263 (1996).
16. J. Zheng, W. N. Zagotta, Stoichiometry and assembly of olfactory cyclic nucleotide-gated channels. *Neuron* **42**, 411–421 (2004).
17. V. Nache *et al.*, Differential regulation by cyclic nucleotides of the CNGA4 and CNGB1b subunits in olfactory cyclic nucleotide-gated channels. *Sci. Signal.* **5**, ra48 (2012).
18. V. Nache *et al.*, Deciphering the function of the CNGB1b subunit in olfactory CNG channels. *Sci. Rep.* **6**, 29378 (2016).
19. C. Waldeck, K. Vocke, N. Ungerer, S. Frings, F. Möhrlen, Activation and desensitization of the olfactory cAMP-gated transduction channel: Identification of functional modules. *J. Gen. Physiol.* **134**, 397–408 (2009).
20. J. Bradley, W. Bönigk, K.-W. Yau, S. Frings, Calmodulin permanently associates with rat olfactory CNG channels under native conditions. *Nat. Neurosci.* **7**, 705–710 (2004).
21. J. Bradley, D. Reuter, S. Frings, Facilitation of calmodulin-mediated odor adaptation by cAMP-gated channel subunits. *Science* **294**, 2176–2178 (2001).
22. W. Bönigk *et al.*, The native rat olfactory cyclic nucleotide-gated channel is composed of three distinct subunits. *J. Neurosci.* **19**, 5332–5347 (1999).
23. E. R. Liman, L. B. Buck, A second subunit of the olfactory cyclic nucleotide-gated channel confers high sensitivity to cAMP. *Neuron* **13**, 611–621 (1994).
24. J. Bradley, J. Li, N. Davidson, H. A. Lester, K. Zinn, Heteromeric olfactory cyclic nucleotide-gated channels: A subunit that confers increased sensitivity to cAMP. *Proc. Natl. Acad. Sci. U.S.A.* **91**, 8890–8894 (1994).
25. K. Matulef, W. N. Zagotta, Cyclic nucleotide-gated ion channels. *Annu. Rev. Cell Dev. Biol.* **19**, 23–44 (2003).
26. G. R. Tibbs, D. T. Liu, B. G. Leypold, S. A. Siegelbaum, A state-independent interaction between ligand and a conserved arginine residue in cyclic nucleotide-gated channels reveals a functional polarity of the cyclic nucleotide binding site. *J. Biol. Chem.* **273**, 4497–4505 (1998).
27. D. Jiang *et al.*, Structure of the cardiac sodium channel. *Cell* **180**, 122–134.e10 (2020).
28. J. Wu *et al.*, Structure of the voltage-gated calcium channel Cav1.1 complex. *Science* **350**, aad2395 (2015).
29. D. Colquhoun, A. G. Hawkes, "The principles of the stochastic interpretation of ion-channel mechanisms" in *Single-Channel Recording*, B. Sakmann, E. Neher, Eds. (Springer US, Boston, MA, 1995), pp. 397–482.
30. M. F. Perutz, A. J. Wilkinson, M. Paoli, G. G. Dodson, The stereochemical mechanism of the cooperative effects in hemoglobin revisited. *Annu. Rev. Biophys. Biomol. Struct.* **27**, 1–34 (1998).
31. K. Benndorf, S. Thon, E. Schulz, Unraveling subunit cooperativity in homotetrameric HCN2 channels. *Biophys. J.* **103**, 1860–1869 (2012).
32. D. E. Koshland Jr, G. Némethy, D. Filmer, Comparison of experimental binding data and theoretical models in proteins containing subunits. *Biochemistry* **5**, 365–385 (1966).
33. D. E. Koshland Jr, K. Hamadani, Proteomics and models for enzyme cooperativity. *J. Biol. Chem.* **277**, 46841–46844 (2002).
34. A. Levitzki, D. E. Koshland Jr, Negative cooperativity in regulatory enzymes. *Proc. Natl. Acad. Sci. U.S.A.* **62**, 1121–1128 (1969).
35. N. Wongsamitkul *et al.*, Quantifying the cooperative subunit action in a multimeric membrane receptor. *Sci. Rep.* **6**, 20974 (2016).
36. M. R. Sunkara, T. Schwabe, G. Ehrlich, J. Kusch, K. Benndorf, All four subunits of HCN2 channels contribute to the activation gating in an additive but intricate manner. *J. Gen. Physiol.* **150**, 1261–1271 (2018).
37. V. Nache *et al.*, Activation of olfactory-type cyclic nucleotide-gated channels is highly cooperative. *J. Physiol.* **569**, 91–102 (2005).
38. Y. Song *et al.*, High-resolution comparative modeling with RosettaCM. *Structure* **21**, 1735–1742 (2013).
39. R. F. Alford *et al.*, An integrated framework advancing membrane protein modeling and design. *PLoS Comput. Biol.* **11**, e1004398 (2015).
40. M. Li *et al.*, Structure of a eukaryotic cyclic-nucleotide-gated channel. *Nature* **542**, 60–65 (2017).
41. N. G. Shuart, Y. Haitin, S. S. Camp, K. D. Black, W. N. Zagotta, Molecular mechanism for 3:1 subunit stoichiometry of rod cyclic nucleotide-gated ion channels. *Nat. Commun.* **2**, 457 (2011).
42. D. Colquhoun, K. A. Dowsland, M. Beato, A. J. R. Plested, How to impose microscopic reversibility in complex reaction mechanisms. *Biophys. J.* **86**, 3510–3518 (2004).
43. W. H. Press, S. A. Teukolsky, W. T. Vetterling, B. P. Flannery, *Numerical Recipes in C: The Art of Scientific Computing* (Cambridge University Press, New York, ed. 2, 2002).